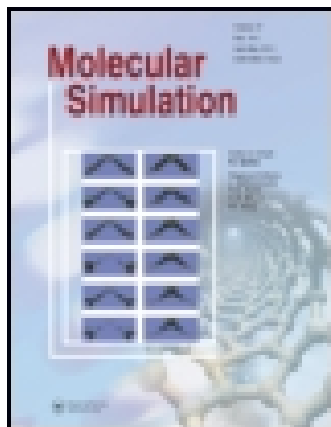


This article was downloaded by: [RMIT University]

On: 27 August 2015, At: 01:35

Publisher: Taylor & Francis

Informa Ltd Registered in England and Wales Registered Number: 1072954 Registered office: 5 Howick Place, London, SW1P 1WG



## Molecular Simulation

Publication details, including instructions for authors and subscription information:

<http://www.tandfonline.com/loi/gmos20>

### Constructing ab initio models of ultra-thin Al-AIO<sub>x</sub>-Al barriers

T.C. DuBois<sup>a</sup>, M.J. Cyster<sup>a</sup>, G. Opletal<sup>a</sup>, S.P. Russo<sup>a</sup> & J.H. Cole<sup>a</sup>

<sup>a</sup> Chemical and Quantum Physics, School of Applied Sciences, RMIT University, Melbourne 3001, Australia

Published online: 26 Aug 2015.



[Click for updates](#)

To cite this article: T.C. DuBois, M.J. Cyster, G. Opletal, S.P. Russo & J.H. Cole (2015): Constructing ab initio models of ultra-thin Al-AIO<sub>x</sub>-Al barriers, *Molecular Simulation*, DOI: [10.1080/08927022.2015.1068941](https://doi.org/10.1080/08927022.2015.1068941)

To link to this article: <http://dx.doi.org/10.1080/08927022.2015.1068941>

PLEASE SCROLL DOWN FOR ARTICLE

Taylor & Francis makes every effort to ensure the accuracy of all the information (the "Content") contained in the publications on our platform. However, Taylor & Francis, our agents, and our licensors make no representations or warranties whatsoever as to the accuracy, completeness, or suitability for any purpose of the Content. Any opinions and views expressed in this publication are the opinions and views of the authors, and are not the views of or endorsed by Taylor & Francis. The accuracy of the Content should not be relied upon and should be independently verified with primary sources of information. Taylor and Francis shall not be liable for any losses, actions, claims, proceedings, demands, costs, expenses, damages, and other liabilities whatsoever or howsoever caused arising directly or indirectly in connection with, in relation to or arising out of the use of the Content.

This article may be used for research, teaching, and private study purposes. Any substantial or systematic reproduction, redistribution, reselling, loan, sub-licensing, systematic supply, or distribution in any form to anyone is expressly forbidden. Terms & Conditions of access and use can be found at <http://www.tandfonline.com/page/terms-and-conditions>

## SPECIAL ISSUE DEDICATED TO THE MEMORY OF PROFESSOR IAN K. SNOOK (1945–2013)

### Constructing *ab initio* models of ultra-thin Al–AlO<sub>x</sub>–Al barriers

T.C. DuBois\*, M.J. Cyster, G. Opletal, S.P. Russo and J.H. Cole

Chemical and Quantum Physics, School of Applied Sciences, RMIT University, Melbourne 3001, Australia

(Received 6 March 2015; final version received 30 June 2015)

The microscopic structure of ultra-thin oxide barriers often plays a major role in modern nano-electronic devices. In the case of superconducting electronic circuits, their operation depends on the electrical nonlinearity provided by one or more such oxide layers in the form of ultra-thin tunnel barriers (also known as Josephson junctions). Currently available fabrication techniques manufacture an amorphous oxide barrier, which is attributed as a major noise source within the device. The nature of this noise is currently an open question and requires both experimental and theoretical investigation. Here, we present a methodology for constructing atomic-scale computational models of Josephson junctions using a combination of molecular mechanics, empirical and *ab initio* methods. These junctions consist of ultra-thin amorphous aluminium-oxide layers sandwiched between crystalline aluminium. The stability and structure of these barriers as a function of density and stoichiometry are investigated, which we compare with experimentally observed parameters.

**Keywords:** Josephson junction; ultra-thin barrier; amorphous structure simulation

#### 1. Introduction

Josephson junctions: ultra-thin insulating layers sandwiched between layers of superconducting metal, are the fundamental building blocks of the next generation of quantum electronics. Examples include superconducting quantum-bits,[1–5] low power Rapid-Single-Flux-Quantum circuits,[6] Superconducting Quantum Interference Devices [7] and nonlinear elements for single quanta microwave electronics.[8–12] In all these cases, Josephson junctions provide the nonlinear element that allows quantum effects to manifest in the voltage, current or magnetic flux signatures of these circuits. Recent work on superconducting qubits [13,14] has shown that a key limiting factor in quantum electronics is the existence of loss mechanisms, which can be traced to material defects in the oxide coating (and protecting) the metallic circuits, as well as the oxide which forms the Josephson junction tunnel barrier. Recent experimental probes of so-called ‘strongly coupled’ defects [15–17] have shown that they can be individually addressed and manipulated, and mostly likely reside within the junction.[18] It is therefore fundamentally important to identify and ideally remove these defects as a source of loss and imperfection in quantum circuits.

From a quantum simulation point of view, this is not a trivial problem. The oxide barrier of a junction is amorphous, so crystalline symmetries cannot be used to reduce the state space. Added to this is the far more fundamental issue that we currently do not understand what forms the defects of interest. Various microscopic models exist, including

hydrogenic dangling bonds,[19–22] charged surface states [23,24] and delocalisation of the oxygen atoms themselves. [25,26] As well as atomistic models, a range of effective defect state models also exist such as phonon dressing of electronic states,[27] metal–insulator gap states [23] and Andreev bound state models.[28] One possible way of distinguishing between these options is to develop complete atomistic models of the Josephson junction and study the configuration of the amorphous layer. Forming such atomistic models using molecular mechanics and *ab initio* methods is the focus of this paper.

#### 2. The Josephson junction formation process

Josephson junctions may be constructed from any superconducting material with any insulating or non-superconducting metal barrier to invoke a weak link coupling. A popular material choice involves the use of aluminium as the superconducting material, and an amorphous oxide layer as an insulating barrier.

Shadow evaporation is a common technique used to fabricate a system such as this, where two metallic layers are deposited from different angles with an intervening oxidation step. This is usually performed using a Dolan [29] bridge, which obscures part of the substrate during each metal deposition step. It has more recently been shown that junction fabrication can be performed without the requirement of this bridge.[30] Regardless of the process chosen, the oxidation of the aluminium does not

\*Corresponding author. Email: [tim.dubois@tcqp.science](mailto:tim.dubois@tcqp.science)

result in a set of crystalline monolayers, but a non-uniform amorphous layer varying in stoichiometry,[31,32] density [33] and thickness [34–36] (nominally  $\sim 2$  nm). Although epitaxial growth of aluminium-oxide barriers has been demonstrated,[37] this technique is not yet mainstream as it is considerably more difficult than conventional shadow mask evaporation. It is therefore the amorphous oxide formation which needs to be investigated predominantly, in order to obtain results from simulation which are applicable to future fabrication work.

Simulating oxide layer growth is in general a difficult problem as the time scale of the oxide growth ( $\sim$ minutes) is many orders of magnitude greater than typically achievable molecular dynamics time scales (ps–ns). One standard approach is to perform the simulation at elevated temperatures and gas pressures ( $\geq 1$  atm).[38–40] This accelerates the oxidation process, making the computation feasible on current high-performance computing infrastructure. However, it also removes the simulation from the reality of experimental junction formation, where pressures range between  $10^{-9}$  and  $10^{-3}$  atm.[41–43] It remains to be seen whether any fundamental physics is neglected by adopting this approximation.

An alternative approach is to form an amorphous layer via direct melt and quench.[44,45] This method has the advantage of computational simplicity and speed, however the resulting layers are not necessarily representative of the true physical situation and therefore benchmarking against other methods and experiment is critical. Generating stoichiometry or density gradients across an artificial junction is not something that can be simulated directly using this process, so to investigate the effect of these properties, a number of constant density and stoichiometry models were produced. A more sophisticated method, closely mimicking the oxygen deposition process and examining the effects of layer thickness will be considered in future work.

### 3. Model construction

To obtain realistic, high precision atomic positions, computational models of the junction were created using a combination of molecular mechanics and density functional theory (DFT). A  $4 \times 4 \times 5$  supercell of bulk aluminium representing both the top and bottom slabs was relaxed in the DFT code VASP [46–48] using a projector-augmented wave (PAW) potential,[49,50] obtaining a  $16.168 \times 16.168 \times 20.183$  Å cell. Exchange–correlation interactions were evaluated using the PBE functional [51]; a  $7 \times 7 \times 7$   $\Gamma$  centred Monkhorst Pack K point mesh and a plane wave cutoff of 250 eV.

Formation of the amorphous  $\text{AlO}_x$  layers required a number of preparation steps to accurately represent experimental results. The low temperature and pressure phase of aluminium oxide (commonly referred to as corundum or  $\alpha\text{-Al}_2\text{O}_3$ ) was used as a basis for all the

constructed junction models. Experimental investigations of stoichiometry suggest, in general, an oxygen deficiency with oxide O/Al ratios varying between 0.6 and 1.4,[32] which are highly dependent on the fabrication process. In response to this, we construct models with four stoichiometries:  $\text{AlO}_{0.8}$ ,  $\text{AlO}_{1.0}$ ,  $\text{AlO}_{1.25}$  and  $\text{AlO}_{1.5}$ . The oxide density may also be an important formation variable. For simplicity we identify oxide density in multiples of the (average) corundum density:  $4.05 \text{ g/cm}^3$ , and construct junctions with 0.5, 0.625, 0.75, 0.875 and 1.0 density multiples for each stoichiometry listed above. A value of  $3.2 \text{ g/cm}^3$  is typical [33] (which corresponds to a density multiple of 0.8), although theoretical predictions suggest altering the density of this barrier may suppress noise sources of the junction.[25]

Using  $\text{AlO}_{1.25}$  with a density multiple of 0.75 as an example, a  $6 \times 6 \times 1$  supercell of corundum was geometry optimised in the software package GULP,[52] employing the empirical Streitz–Mintmire potential [53] which can capture the variable oxygen charge states when present in a predominantly metallic environment. This capability is particularly important here, as a Josephson junction has two metal–oxide interfaces. This large superstructure was required due to the trigonal nature of the lattice, as it was then cut down such that the  $xy$  plane of the bulk aluminium slab could be covered. A non-periodic slab of corundum measuring  $16.168 \times 16.168 \times 11.982$  Å was the result of this process. Oxygen atoms were randomly removed from the corundum lattice until the appropriate stoichiometry of  $\text{AlO}_{1.25}$  was obtained and the cell was shortened in the  $z$ -direction to achieve a 0.75 fractional multiple of the corundum density. These changes add quite a lot of force onto the structure, so a geometry optimisation (in GULP) was undertaken at this stage to minimise energy contributions. To simulate the oxygen deposition phase and generate the amorphous nature of these layers, the structure was then annealed using NVT molecular dynamics at 3000 K with a 1 fs step size for  $3 \mu\text{s}$  and quenched to 350 K over a  $1.5 \mu\text{s}$  period.

The  $\text{AlO}_{1.25}$  layer was inserted between two bulk Al supercells described above with 0.5 Å of vacuum space on each side. The junction was further annealed to simulate a metal–metal–oxide interface reconstruction using VASP NVT Molecular Dynamics at 300 K until equilibrium was reached (approximately 250 ionic steps), then geometry optimised using a  $2 \times 2 \times 1$   $\Gamma$  centred Monkhorst Pack K point mesh and a 450 eV plane wave cutoff to obtain the final model, depicted in Figure 1.

For comparison, junctions were also modelled without the added computational overhead of DFT by solely employing GULP and the Streitz–Mintmire potential. The construction process of these models matches the procedure above, but interchanges the *ab initio* optimisations of the oxide layer with an empirical framework.

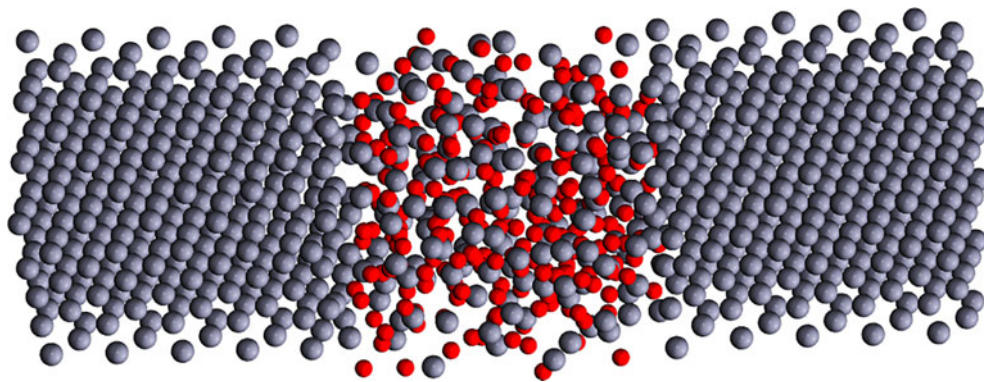


Figure 1. (Colour online) Model of a Josephson junction comprised of aluminium (grey) and oxygen (red). Two superconducting regions composed only of aluminium, separated by an amorphous  $\text{AlO}_{1.25}$  barrier with a density 0.75 times that of corundum.

#### 4. Results and discussion

To validate our models against experimental observations, we perform a number of statistical tests to scrutinise the structures. First, we must ensure that the oxide layer of each junction is in fact amorphous in nature. We employ a projected radial distribution function

$$G(r) = \lim_{dr \rightarrow 0} \frac{p(r)}{4\pi(N_{\text{pairs}}/V)r^2 dr}, \quad (1)$$

where  $r$  is the distance between a pair of particles,  $p(r)$  is the average number of atom pairs found at a distance between  $r$  and  $r + dr$ ,  $V$  is the total volume of the system, and  $N_{\text{pairs}}$  is the number of unique pairs of atoms.[54] This function was calculated for each stoichiometry and density configuration using oxygen as the reference species, and aluminium atoms in the amorphous region along with the superconducting bulk as the projection species. Figure 2 depicts the results of this analysis.

A major peak is visible centred around  $1.85 \text{ \AA}$ , which corresponds to convolution of the two Al–O bond distances,  $1.852$  and  $1.971 \text{ \AA}$  of the corundum crystal.[55] For a crystalline  $G(r)$  this peak is deconvolved to two delta functions (see Figure 2 and the discussion below), where here we see a broadening of the statistics and hence differences in neighbour distances: diverging from a crystalline form. Moving away from this peak to larger distance separations, we see the statistics tending towards a uniform result similar to what a liquid would produce under this analysis. These two features represent an amorphous system quite well, as close range order suggests a connection to the crystalline form whilst long-range order no longer agrees with such periodic conditions. It's also significant to note that we do not observe neighbours closer than  $\sim 1.5 \text{ \AA}$  which is a good indication that the models do not have non-physical neighbour forces acting on atoms.

Most importantly, this trend is almost uniform across all the modelled junctions, which indicate the process

outlined in Section 3 is capable of producing amorphous oxides whilst varying other physical parameters of the system. An evolution of the important steps in the procedure is depicted in Figure 2.

The corundum  $G(r)$  (thin, grey) is a complicated structure due to the 30 atom unit cell of the crystal, however it is clear from this figure where much of the amorphous structure originates from. Specifically the  $1.852$  and  $1.971 \text{ \AA}$  Al–O bond distance contributions and the void in the  $2\text{--}3 \text{ \AA}$  range. After the melt/quench phase of the procedure the lattice still appears liquid-like (dash dotted, green). Whilst the quench cycle minimises the possibility of atoms position very close to one another due

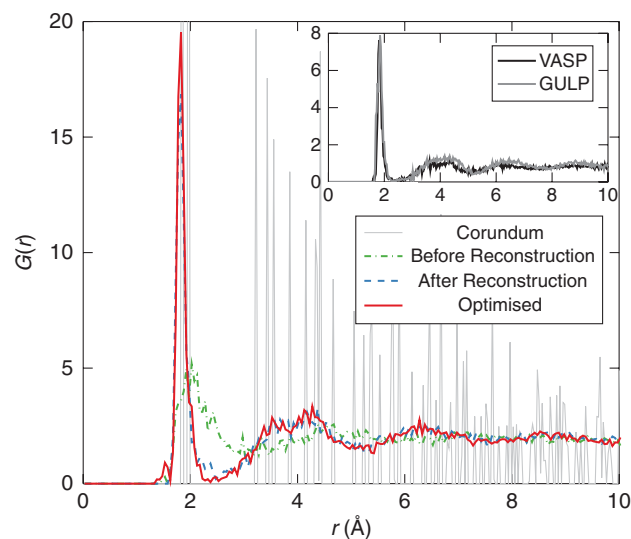


Figure 2. (Colour online) Evolution of the oxygen projected radial distribution function  $G(r)$ . Crystalline corundum (thin, grey); metal–metal–oxide interface reconstruction before (dash dotted, green) and after (dashed, blue); final optimised geometry (thick, red). Inset: Oxygen projected  $G(r)$  computed using *ab initio* (VASP) and empirical (GULP) methods, showing no statistically significant differences.

to an excess of kinetic energy, it still appears to exhibit liquid behaviour. This may be a shortcoming of the Streitz–Mintmire potentials ability to capture the relevant physics, however this is rectified after the metal–metal–oxide interface reconstruction is completed (dashed, blue) using the *ab initio* methods. Finally, the geometry optimisation (thick, red) yields a smoother  $1.85 \text{ \AA}$  peak and recovers some of the void region around  $2 \text{ \AA}$ .

The inset of Figure 2 compares the optimal  $G(r)$  results for both the VASP and GULP simulations. Whilst these results are very similar, the GULP simulation actually produces a drastically different final structure. We find under GULP simulation that stoichiometric ratios higher than 1:1 are not stable and oxygen atoms diffuse into the metallic regions until a stoichiometric ratio of at most 1:1 is achieved. As a result of this excess oxygen diffusion, the junction width can increase by up to 30% or more over the course of the simulation. At high densities and stoichiometries (higher than typical amorphous alumina) some expansion of the oxide region is also seen in the *ab initio* simulations, although this effect is much less pronounced. Higher oxygen mobility in GULP could be attributed to shortcomings of the empirical potential, but we see very little increase in oxide distribution during the optimisation phase – suggesting that the details of the Nosé–Hoover thermostat routine employed during the MD simulation may play a role.

The total energy of a computational model is a good indication of the structure’s electronic stability. Due to the stoichiometry changes invoked in the oxygen-depleted models, not all structures have the same number of atoms. This gives structures with more atoms (such as  $\text{AlO}_{1.5}$ )

additional electronegativity which in turn results in a deeper potential well and a large total energy. In order to be able to validly compare systems of different stoichiometry, we normalise the total energy of each system by a factor  $|F|$ .  $F = \sum_k \mu_k N_k$  is calculated as the linear combination of the number of atoms of chemical species  $k$  ( $N_k$ ) by the chemical potential of that species ( $\mu_k$ ), where  $k = \{\text{Al}, \text{O}\}$ . The chemical potential for aluminium,  $\mu_{\text{Al}}$  was obtained by calculating the DFT total energy of a  $4 \times 4 \times 5$  supercell of bulk Al and dividing by the number of atoms in the supercell. Similarly the chemical potential of oxygen was obtained from calculating the DFT total energy of a  $2 \times 2 \times 2$  supercell of bulk  $\text{Al}_2\text{O}_3$  using  $\mu_{\text{O}} = (\mu_{\text{Al}_2\text{O}_3} - 2\mu_{\text{Al}})/3$ , where  $\mu_{\text{Al}_2\text{O}_3}$  is the total energy of a molecular unit of  $\text{Al}_2\text{O}_3$ . The factor  $F$  (essentially the free energy at  $T = 0$ ) effectively allows one to partition the total energy of the system using the chemical potentials of each component species, as a means to compare the energies of systems with differing number of chemical components.

It is clear from Figure 3 that stoichiometry plays a larger role in energy minimisation than density, and that the structures would prefer additional oxygen to minimise internal forces. This suggests that fabrication processes that generate oxygen deficiencies may be inviting the inclusion of alien species or oxygenic site hopping in an attempt to rectify this offset.

Density changes seem to alter the energy contribution marginally. Minimum energies correspond to density multiples between 0.6 and 0.75, slightly lower than typical constructions of  $3.2 \text{ g/cm}^3$  [33] (an 0.8 density multiple); which may indicate another method of experimentally optimising the junction formation process.

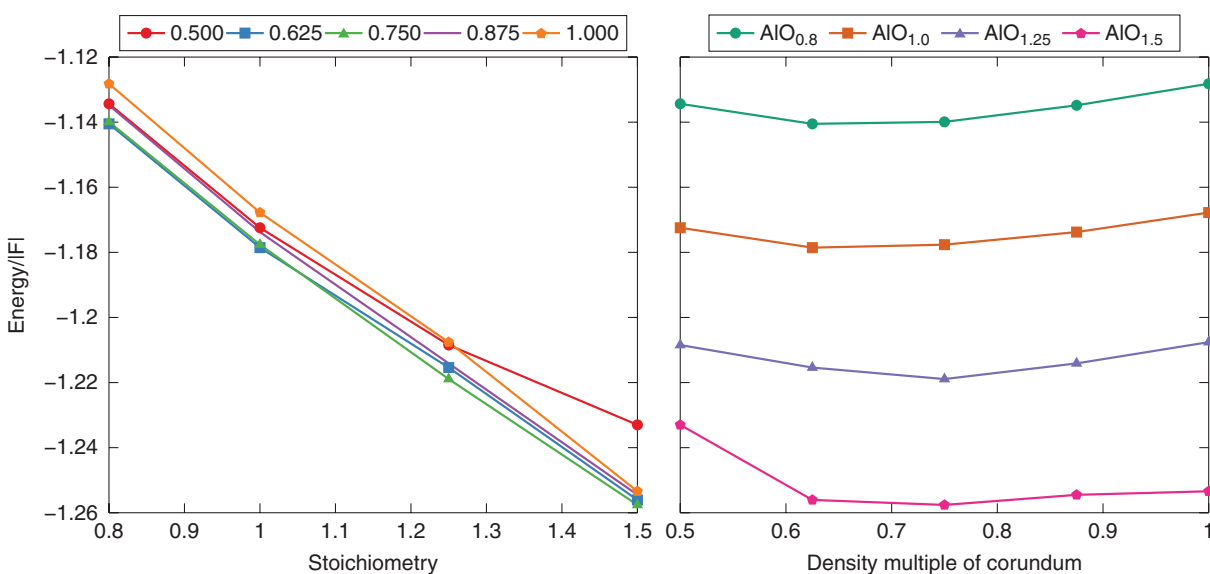


Figure 3. (Colour online) Normalised total energy for various junction models with stoichiometry (left) and density (right). Although the energy is strongly dependent on stoichiometry, we see a trend to optimal densities of approximately 75% of the density of corundum.

Coordination number is a useful metric which allows for some insight into both the crystallinity of the structures being analysed, and their similarity to fabricated junctions. For instance, in the corundum structure every aluminium ion is coordinated with six oxygen ions. In amorphous alumina, the proportion of 6-coordinated aluminium compared with 4-coordinated aluminium is an experimentally accessible quantity and has been reported on previously.[56] However, in order to establish this ratio it is assumed that there is a bimodal distribution of octahedral ( $\text{AlO}_6$ ) and tetrahedral ( $\text{AlO}_4$ ) coordination. Ratios of  $\text{AlO}_6 : \text{AlO}_4$  are quoted in a range from 80:20 to 30:70, depending on the method by which the oxide layer was formed.[57] More modern techniques using nuclear magnetic

resonance are also able to resolve the  $\text{AlO}_5$  coordination.[58]

Figure 4 shows the distribution of oxygen coordination about aluminium as a function of density and stoichiometry. These results are calculated using an Al–O bond length cutoff of  $2.5 \text{ \AA}$ , which corresponds to the first minimum after the nearest neighbour peak in the  $G(r)$  (see Figure 2). As one would expect, the coordination number (for Al–O bonding) increases with increasing density or stoichiometry. We also note that there exists a reasonable proportion of 2- and 3-coordinated aluminium atoms, which persists at high density and stoichiometry. In order to compare directly to previous experimental and theoretical work, we compute the ratio of 4-, 5- and 6-coordination for Al–O bonding, matching the stoichi-

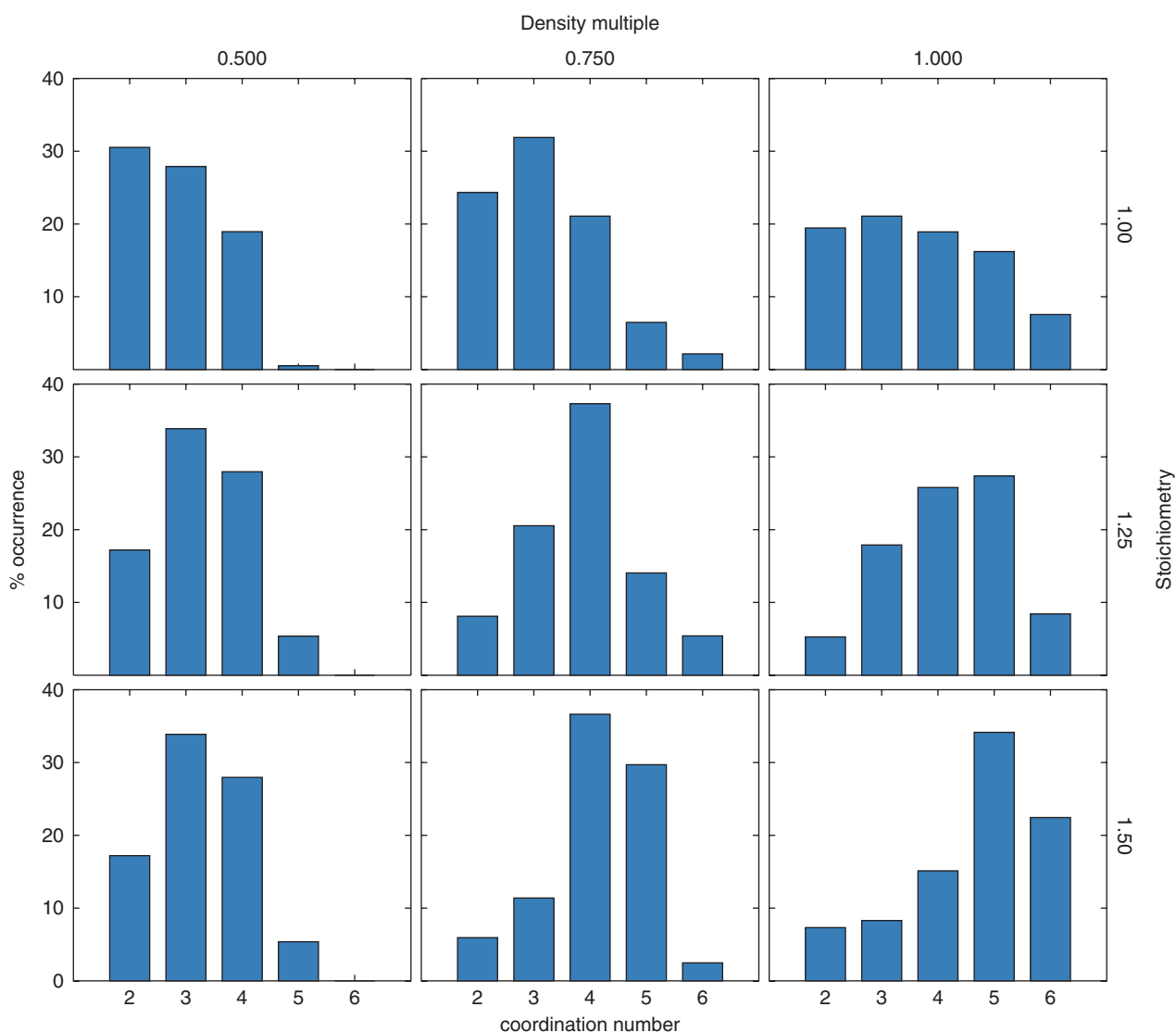


Figure 4. (Colour online) Distribution of oxygen coordination about aluminium as a function of density and stoichiometry, showing a tendency to higher coordination number with increasing density or stoichiometry.

Table 1. Relative proportions of 4-, 5- and 6-coordinated aluminium atoms within the oxide layer for a density of 0.75 and stoichiometry of 1.5.

	4 (%)	5 (%)	6 (%)
VASP (before optimisation)	57	39	4
VASP (after optimisation)	53	43	4
Lee et al. [58]; experiment	$55 \pm 3$	$42 \pm 3$	$3 \pm 2$
Momida et al. [59]; theory	60.4	29.2	10.4

ometry of 1.5 and assuming the density multiple closest to experimental values (0.750). The results are presented in Table 1. We observe excellent agreement, both before and after the *ab initio* optimisation.

## 5. Conclusions

Precise computational models of Josephson junctions are becoming crucial to efforts to reduce dissipation and loss in superconducting circuits. The limits of computational resources mean that full *ab initio* models are computationally intractable. However, a combination of *ab initio* and empirical models holds promise for developing flexible and efficient simulation approaches. We have constructed models of amorphous aluminium-oxide barriers, sandwiched between crystalline aluminium. Through comparisons with both previous theoretical analysis and experimental measurements, we have shown that the resulting structures are representative of those fabricated experimentally. The structure of such junctions can be used as input conditions to potential microscopic models for either charge or magnetic defects in Josephson junctions. Through this approach, free parameters in existing phenomenological defect models can be determined via information directly obtained from the atomic positions.

## Disclosure statement

No potential conflict of interest was reported by the authors.

## Funding

This research was supported under the Australian Research Council's Discovery Projects funding scheme [project number DP140100375]. Computational resources were provided at the NCI National Facility systems at the Australian National University through the National Computational Merit Allocation Scheme supported by the Australian Government.

## References

[1] Clarke J, Cleland AN, Devoret MH, Esteve D, Martinis JM. Quantum mechanics of a macroscopic variable: the phase difference of a Josephson junction. *Science*. 1988;239:992–997.  
 [2] Martinis JM, Nam S, Aumentado J, Urbina C. Rabi oscillations in a large Josephson-junction qubit. *Phys Rev Lett*. 2002;89:117901.

[3] Plourde BLT, Robertson TL, Reichardt PA, Hime T, Linzen S, Wu C-E, John Clarke Flux qubits and readout device with two independent flux lines. *Phys Rev B Condens Matter Mater Phys*. 2005;72:1–4.  
 [4] Deppe F, Mariani M, Menzel EP, Saito S, Kakuyanagi K, Tanaka H, Meno T, Semba K, Takayanagi H, Gross R. Phase coherent dynamics of a superconducting flux qubit with capacitive bias readout. *Phys Rev B Condens Matter Mater Phys*. 2007;76:1–19.  
 [5] Schreier JA, Houck AA, Koch J, Schuster DI, Johnson BR, Chow JM, Gambetta JM, Majer J, Frunzio L, Devoret MH, Girvin SM, Schoelkopf RJ. Suppressing charge noise decoherence in superconducting charge qubits. *Phys Rev B*. 2008;77:180502.  
 [6] Mukhanov O, Semenov V, Likharev K. Ultimate performance of the RSFQ logic circuits. *IEEE Trans Magnetics* 1987;23:759–762.  
 [7] Clarke J. SQUID fundamentals. In: Weinstock H, editor. *Squid sensors: fundamentals, fabrication and applications*. Springer, Netherlands, 1996.  
 [8] Astafiev O, Inomata K, Niskanen AO, Yamamoto T, Pashkin YA, Nakamura Y, Tsai JS. Single artificial-atom lasing. *Nature*. 2007;449:588–590.  
 [9] Astafiev O, Zagoskin AM, Abdumalikov AA, Pashkin YA, Yamamoto T, Inomata K, Nakamura Y, Tsai JS. Resonance fluorescence of a single artificial atom. *Science (New York, NY)*. 2010;327:840–843.  
 [10] Wilson CM, Johansson G, Pourkabirian A, Simoen M, Johansson JR, Duty T, Nori F, Delsing P. Observation of the dynamical Casimir effect in a superconducting circuit. *Nature*. 2011;479:376–379.  
 [11] Hoi IC, Kockum AF, Palomaki T, Stace TM, Fan B, Tornberg L, Sathyamoorthy SR, Johansson G, Delsing P, Wilson CM. Giant cross-kerr effect for propagating microwaves induced by an artificial atom. *Phys Rev Lett*. 2013;111:2–6.  
 [12] Hoi I-C, Wilson CM, Johansson G, Lindkvist J, Peropadre B, Palomaki T, Delsing P. Microwave quantum optics with an artificial atom in one-dimensional open space. *New J Phys*. 2013;15:025011.  
 [13] Dutta P, Horn P. Low-frequency fluctuations in solids:  $1/f$  noise. *Rev Mod Phys*. 1981;53:497–516.  
 [14] Shnirman A, Schön G, Martin I, Makhlin Y. Low- and high-frequency noise from coherent two-level systems. *Phys Rev Lett*. 2005;94:127002.  
 [15] Neeley M, Ansmann M, Bialczak RC, Hofheinz M, Katz N, Lucero E, O'Connell A, Wang H, Cleland AN, Martinis JM. Process tomography of quantum memory in a Josephson-phase qubit coupled to a two-level state. *Nat Phys*. 2008;4:523–526.  
 [16] Lupaşcu A, Bertet P, Driessen EFC, Harmans CJPM, Mooij JE. One- and two-photon spectroscopy of a flux qubit coupled to a microscopic defect. *Phys Rev B*. 2009;80:172506.  
 [17] Lisenfeld J, Müller C, Cole JH, Bushev P, Lukashenko A, Shnirman A, Ustinov AV. Measuring the temperature dependence of individual two-level systems by direct coherent control. *Phys Rev Lett*. 2010;105:230504.  
 [18] Lacquaniti V, Belogolovskii M, Cassiago C, De Leo N, Fretto M, Sosso A. Universality of transport properties of ultrathin oxide films. *New J Phys*. 2012;14:023025.  
 [19] Martinis JM, Cooper KB, McDermott R, Steffen M, Ansmann M, Osborn KD, Cicak K, Oh S, Pappas DP, Simmonds RW, Yu C. Decoherence in Josephson qubits from dielectric loss. *Phys Rev Lett*. 2005;95:210503.  
 [20] Jameson JR, Ngo D, Benko C, McVittie JP, Nishi Y, Young BA. Dielectric relaxation study of hydrogen exposure as a source of two-level systems in  $\text{Al}_2\text{O}_3$ . *J Non-Crystalline Solids*. 2011;35710:2148–2151.  
 [21] Holder AM, Osborn KD, Lobb CJ, Musgrave CB. Bulk and surface tunneling hydrogen defects in alumina. *Phys Rev Lett*. 2013;111:065901.  
 [22] Gordon L, Abu-Farsakh H, Janotti A, Van de Walle CG. Hydrogen bonds in  $\text{Al}_2\text{O}_3$  as dissipative two-level systems in superconducting qubits. *Sci Rep*. 2014;4:7590.  
 [23] Choi S, Lee D-H, Louie SG, Clarke J. Localization of metal-induced gap states at the metal–insulator interface: origin of flux noise in SQUIDs and superconducting qubits. *Phys Rev Lett*. 2009;103:197001.  
 [24] Lee D, DuBois J, Lordi V. Identification of the local sources of paramagnetic noise in superconducting qubit devices fabricated on

- $\alpha$ -Al<sub>2</sub>O<sub>3</sub> substrates using density-functional calculations. Phys Rev Lett. 2014;112:017001.
- [25] DuBois TC, Per MC, Russo SP, Cole JH. Delocalized oxygen as the origin of two-level defects in Josephson junctions. Phys Rev Lett. 2013;110:077002.
- [26] DuBois TC, Russo SP, Cole JH. Atomic delocalization as a microscopic origin of two-level defects in Josephson junctions. New J Phys. 2015;17:023017.
- [27] Agarwal K, Martin I, Lukin MD, Demler E. Polaronic model of two-level systems in amorphous solids. Phys Rev B. 2013;87:144201.
- [28] de Sousa R, Whaley KB, Hecht T, von Delft J, Wilhelm FK. Microscopic model of critical current noise in Josephson-junction qubits: subgap resonances and Andreev bound states. Phys Rev B. 2009;80:094515.
- [29] Dolan GJ. Offset masks for lift-off photoprocessing. Appl Phys Lett. 1977;31:337–339.
- [30] Lecocq F, Pop IM, Peng Z, Matei I, Crozes T, Fournier T, Naud C, Guichard W, Buisson O. Junction fabrication by shadow evaporation without a suspended bridge. Nanotechnology. 2011; 22:315302.
- [31] Park BG, Bae JY, Lee TD. Growth characteristics of Al oxide formed by ozone in magnetic tunnel junctions. J Appl Phys. 2002; 9110:8789.
- [32] Tan E, Mather PG, Perrella AC, Read JC, Buhrman RA. Oxygen stoichiometry and instability in aluminum oxide tunnel barrier layers. Phys Rev B. 2005;71:161401.
- [33] Barbour JC, Copeland RG, Dunn RG, Missert N, Montes LP, Son K-A, Sullivan JP. The electrical properties of native and deposited thin aluminum oxide layers on aluminum: hydration effects. The electrochemical society meeting.
- [34] Gloos K, Koppinen PJ, Pekola JP. Properties of native ultrathin aluminium oxide tunnel barriers. J Phys Condens Matter. 2003; 1510:1733–1746.
- [35] Aref T, Averin A, van Dijken S, Ferring A, Koberidze M, Maisi VF, Nguyen H, Nieminen RM, Pekola JP, Yao LD. Characterization of aluminum oxide tunnel barriers by combining transport measurements and transmission electron microscope imaging. J Appl Phys. 2014;116:1–1.
- [36] Zeng LJ, Nik S, Greibe T, et al. Direct observation of the thickness distribution of ultra thin AlO<sub>x</sub> barrier in Al/AlO<sub>x</sub>/Al Josephson junctions. arXiv:1407.0173, 2014.
- [37] Oh S, Cicak K, Kline JS, Sillanpää MA, Osborn KD, Whittaker JD, Simmonds RW, Pappas DP. Elimination of two level fluctuators in superconducting quantum bits by an epitaxial tunnel barrier. Phys Rev B Condens Matter Mater Phys. 2006;7410:1–4.
- [38] Campbell T, Kalia RK, Nakano A, Vashishta P, Ogata S, Rodgers S. Dynamics of oxidation of aluminum nanoclusters using variable charge molecular-dynamics simulations on parallel computers. Phys Rev Lett. 1999;82:4866–4869.
- [39] Zhou X, Wadley H. Atomistic simulation of AlO<sub>x</sub> magnetic tunnel junction growth. Phys Rev B. 2005;71:054418.
- [40] Hasnaoui A, Politano O, Salazar JM, Aral G, Kalia RK, Nakano A, Vashishta P. Molecular dynamics simulations of the nano-scale room-temperature oxidation of aluminum single crystals. Surf Sci. 2005;579:47–57.
- [41] Morohashi S, Hasuo S. Experimental investigations and analysis for high-quality Nb/Al–AlO<sub>x</sub>/Nb Josephson junctions. J Appl Phys. 1987;6110:4835.
- [42] Kohlstedt H, Hallmanns G, Nevirkovets IP, Gugli D, Heiden C. Preparation and properties of Nb/Al–AlO<sub>x</sub>/Nb multilayers. IEEE Trans Appl Superconductivity. 1993;3:2197–2200.
- [43] Jeurgens LPH, Sloof WG, Tichelaar FD, Mittemeijer EJ. Structure and morphology of aluminium-oxide films formed by thermal oxidation of aluminium. Thin Solid Films. 2002;418:89–101.
- [44] Vashishta P, Kalia RK, Nakano A, Rino JP. Interaction potentials for alumina and molecular dynamics simulations of amorphous and liquid alumina. J Appl Phys. 2008;103:083504.
- [45] Sheng HW, Ma E, Kramer MJ. Relating dynamic properties to atomic structure in metallic glasses. JOM. 2012;64:856–881.
- [46] Kresse G, Hafner J. Norm-conserving and ultrasoft pseudopotentials for first-row and transition elements. J Phys Condens Matter. 1994; 640:8245–8257.
- [47] Kresse G, Furthmüller J. Efficiency of *ab-initio* total energy calculations for metals and semiconductors using a plane-wave basis set. Comput Mater Sci. 1996;6:15–50.
- [48] Kresse G, Furthmüller J, Kresse G. Efficient iterative schemes for *ab initio* total-energy calculations using a plane-wave basis set. Phys Rev B. 1996;54:11169–11186.
- [49] Kresse G, Joubert D, Kresse G. From ultrasoft pseudopotentials to the projector augmented-wave method. Phys Rev B. 1999;59: 1758–1775.
- [50] Blöchl PE. Projector augmented-wave method. Phys Rev B. 1994; 50:17953–17979.
- [51] Perdew JP, Burke K, Ernzerhof M. Generalized gradient approximation made simple. Phys Rev Lett. 1996;77:3865–3868.
- [52] Gale JD, Rohl AL. The general utility lattice program (GULP). Mol Simulat. 2003;29:291–341.
- [53] Streitz F, Mintmire J. Electrostatic potentials for metal&ndash;oxide surfaces and interfaces. Phys Rev B. 1994;50:11996–12003.
- [54] Levine BG, Stone JE, Kohlmeyer A. Fast analysis of molecular dynamics trajectories with graphics processing units-radial distribution function histogramming. J Comput Phys. 2011;230:3556–3569.
- [55] Ishizawa N, Miyata T, Minato I, Marumo F, Iwai S. A structural investigation of  $\alpha$ -Al<sub>2</sub>O<sub>3</sub> at 2170 K. Acta Crystallogr B Struct Crystallogr Crystal Chem. 1980;36:228–230.
- [56] El-mashri SM, Jones RG, Forty AJ. An electron-yield EXAFS study of anodic-oxide and hydrated-oxide films on pure aluminum. Philos Mag A. 1983;48:665–683.
- [57] Bourdillon AJ, El-mashri SM, Forty AJ. Application of TEM extended electron energy loss fine structure to the study of aluminium oxide films. Philos Mag A. 1984;49:341–352.
- [58] Lee SK, Lee SB, Park SY, Yi, YS, Ahn CW. Structure of amorphous aluminum oxide. Phys Rev Lett. 2009;103:4–7.
- [59] Momida H, Nigo S, Kido G, Ohno T. Effect of vacancy-type oxygen deficiency on electronic structure in amorphous alumina. Appl Phys Lett. 2011;98:042102.